Acta Crystallographica Section C
Crystal Structure Communications
ISSN 0108-2701

N-{*N*-[2-(3,5-Difluorophenyl)acetyl]-(*S*)-alanyl}-(*S*)-phenylglycine *tert*-butyl ester (DAPT): an inhibitor of γ-secretase, revealing fine electronic and hydrogen-bonding features

Andrzej Czerwinski,[a] Francisco Valenzuela,[a] Pavel Afonine,[b] Miroslawa Dauter[c]* and Zbigniew Dauter[d]

[a]Peptides International Inc., 11621 Electron Drive, Louisville, KY 40299, USA, [b]Lawrence Berkeley National Laboratory, One Cyclotron Road, Building 64R0121, Berkeley, CA 94720, USA, [c]Basic Research Program, SAIC–Frederick Inc., Synchrotron Radiation Research Section, MCL, NCI, Argonne National Laboratory, Biosciences Division, Building 202, Argonne, IL 60439, USA, and [d]Synchrotron Radiation Research Section, MCL, NCI, Argonne National Laboratory, Biosciences Division, Building 202, Argonne, IL 60439, USA
Correspondence e-mail: dauter@anl.gov

Received 16 September 2010
Accepted 28 October 2010
Online 6 November 2010

The title compound, $C_{23}H_{26}F_2N_2O_4$, is a dipeptidic inhibitor of γ-secretase, one of the enzymes involved in Alzheimer's disease. The molecule adopts a compact conformation, without intramolecular hydrogen bonds. In the crystal structure, one of the amide N atoms forms the only intermolecular N—H···O hydrogen bond; the second amide N atom does not form hydrogen bonds. High-resolution synchrotron diffraction data permitted the unequivocal location and refinement without restraints of all H atoms, and the identification of the characteristic shift of the amide H atom engaged in the hydrogen bond from its ideal position, resulting in a more linear hydrogen bond. Significant residual densities for bonding electrons were revealed after the usual *SHELXL* refinement, and modeling of these features as additional interatomic scatterers (IAS) using the program *PHENIX* led to a significant decrease in the *R* factor from 0.0411 to 0.0325 and diminished the r.m.s. deviation level of noise in the final difference Fourier map from 0.063 to 0.037 e Å^{-3}.

Comment

Alzheimer's disease, a progressive neurodegenerative disorder, is the most prominent contributor to senile dementia, a condition affecting millions of individuals worldwide. The disease is associated with the presence of extracellular plaques and intracellular neurofibrillary tangles in the brains of Alzheimer's sufferers (Goedert & Spillantini, 2006). Amyloid-β plaque peptides are produced as a result of the sequential proteolytic cleavages of a protein precursor, involving β- and γ-secretase enzymes (Chapman *et al.*, 2001). A great amount of effort has been expended in exploring the use of the enzyme inhibitors and modulators aimed at preventing amyloid formation (Wolfe, 2008). An approach based on targeting γ-secretase (Roberts, 2002; Barten *et al.*, 2006; Tomita, 2008) seems to be more promising (Wolfe, 2008) than an approach that has been focused on β-secretase (Vassar, 2002; Schmidt *et al.*, 2006). This research generated a number of potent and specific inhibitors, among them *N*-[*N*-(3,5-difluorophenylacetyl)-*S*-alanyl]-(*S*)-phenylglycine *tert*-butyl ester (DAPT) (Dovey *et al.*, 2001). DAPT, (I), has been shown to block amyloid-β production in human neuronal cultures, and its administration to transgenic mice resulted in the first successful reduction of amyloid level *in vivo* (Dovey *et al.*, 2001; Lanz *et al.*, 2003). Presenilin, a component of the γ-secretase complex, has been reported as a molecular target of DAPT (Morohashi *et al.*, 2006). Besides being a γ-secretase inhibitor, DAPT is also an inhibitor of the Notch signaling pathway, involved in cell proliferation, differentiation and apoptosis (Hansson *et al.*, 2004; Katoh & Katoh, 2007). Due to this inhibition property, future clinical applications of DAPT for Alzheimer's disease treatment are rather unlikely. However, it is still widely used as a valuable tool in a variety of biomedical investigations (Sjolund *et al.*, 2008; Bittner *et al.*, 2009; Huang *et al.*, 2010; Zhu *et al.*, 2010), with new and interesting features and possible novel applications emerging (Grottkau *et al.*, 2009; Loane *et al.*, 2009). To facilitate the rational design of γ-secretase inhibitors with improved properties, we have crystallized and elucidated the structure of DAPT.

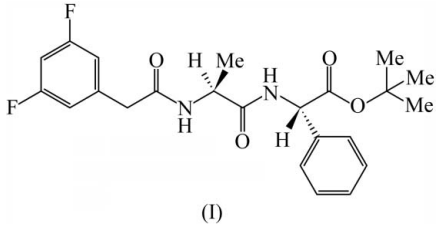

(I)

The single molecule of the DAPT dipeptide in the asymmetric unit of (I) is in a compact conformation (Fig. 1), in which the main-chain torsion angles lie in the allowed regions of the Ramachandran plot, *viz.* $\varphi = -69.43\,(17)^\circ$ and $\psi = -33.53\,(18)^\circ$ for Ala, and $\varphi = -161.83\,(14)^\circ$ and $\psi = 157.57\,(13)^\circ$ for PheGly, so that the former residue corresponds to the α-helical and the latter to the extended β-conformation.

There is only a single intermolecular hydrogen bond between the Ala N20—H group and carbonyl atom O21 of the Ala residue related by translation parallel to *a* (Fig. 2*a*). The remaining N and O atoms of DAPT are not engaged in hydrogen bonds.

All H atoms were identified from the difference Fourier synthesis. Two modes of their refinement were applied, firstly using the customary 'riding' model in geometrically idealized positions utilizing the appropriate rigid-body constraints in *SHELXL* (Sheldrick, 2008), and secondly refining all their

 doi:10.1107/S0108270110044136

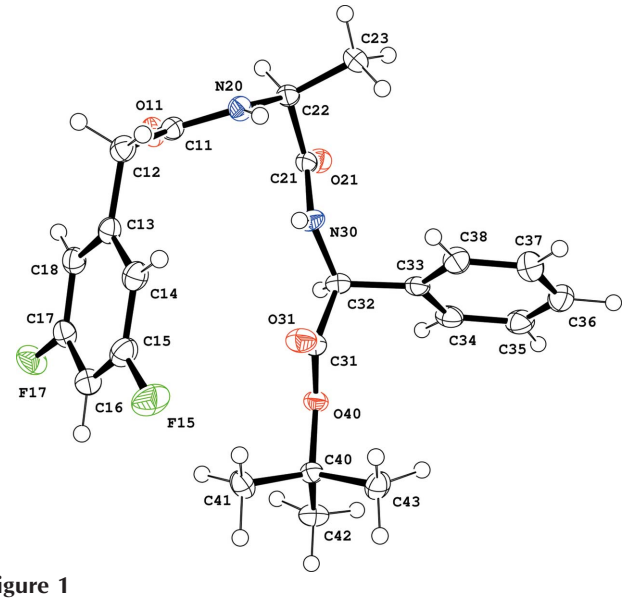

Figure 1
The molecule of DAPT, showing the atom-labeling scheme. Displacement ellipsoids are drawn at the 50% probability level.

positional and isotropic U parameters without any constraints or restraints. The R(all) factors for such constrained and free refinements were comparable (0.0408 and 0.0399, respectively). The root-mean-square deviation (r.m.s.d.) of all 26 bond lengths to all H atoms between the two models was 0.036 Å and the r.m.s.d. of all bond directions was 4.0°, with only one outlier differing by 14.6° from the idealized bond direction. The single outlier corresponds to H201, an H atom of the amide N atom, which is engaged in the only (intermolecular) hydrogen bond in the structure. Its distortion from the direction exactly bisecting the C11—N20—C22 angle is clearly caused by the tendency of the hydrogen bond to be linear (Fig. 2*b*). Excluding it from the statistics of the bond directions resulted in an r.m.s.d. for the 25 bond directions of 2.8°. The model after the nonconstrained refinement of H atoms was accepted as the result of the *SHELXL* minimization.

The difference Fourier synthesis computed at the end of the *SHELXL* refinement showed relatively strong residual electron-density maxima located between bonded atoms (near bond centers) for almost all bonds. These features are due to bonding effects and their visibility is warranted by the combination of three facts: high data resolution, high model quality (low R factor) and low B factors ($B < 5$ Å^2) (Afonine *et al.*, 2004). A multipolar model (Hansen & Coppens, 1978) is appropriate to use in such cases, since it accounts for the effects of atom interations. It has been demonstrated that a simplified interatomic scatterers (IAS) model is capable of producing results of similar quality using fewer refinable parameters (Afonine *et al.*, 2004, 2007). An additional refinement was therefore undertaken with the program *PHENIX* (Afonine *et al.*, 2005), which supports refinement with the IAS option.

The *PHENIX* procedure started with the independent atom model (IAM), which included completely unrestrained refinement of atomic coordinates, anisotropic displacement parameters for non-H atoms and isotropic displacement parameters for H atoms. The occupancies of the H atoms were allowed to refine, to account for the possible effect of H-atom abstraction due to radiation damage (Meents *et al.*, 2009). This resulted in R(all) = 0.0411. For comparison, an analogous

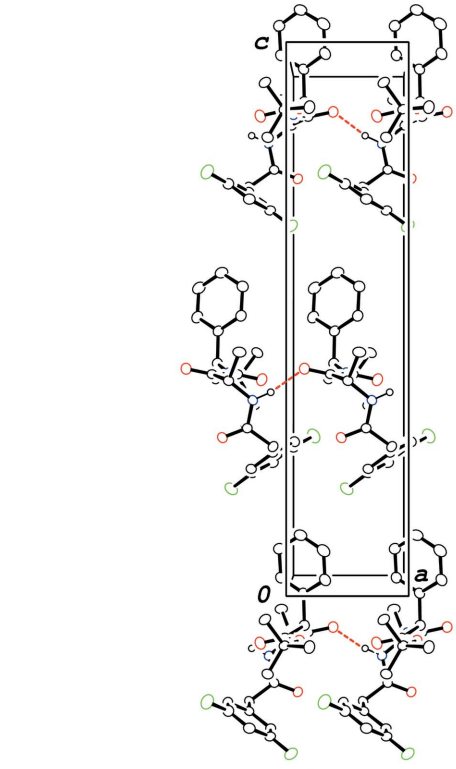

(*a*)

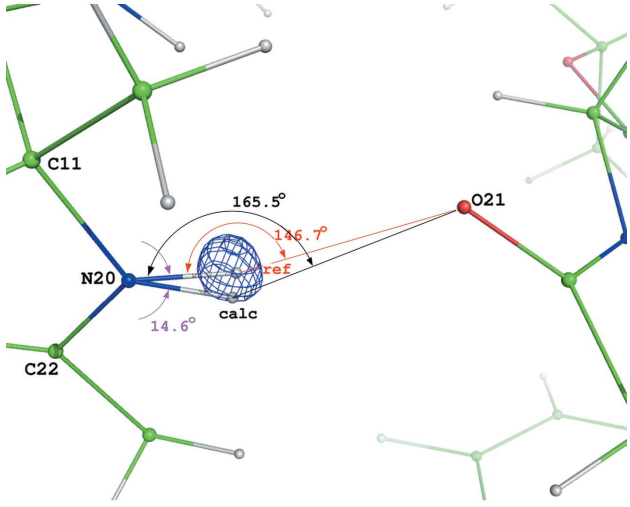

(*b*)

Figure 2
(*a*) The packing of DAPT molecules, viewed along the *b* direction. The only intermolecular hydrogen bond is marked as dashed lines. (*b*) A close-up of the N20—H···O21 hydrogen bond, with atom H210 shown in two options, *viz.* in the calculated idealized position and after free refinement without constraints. The atom labeled O21 is a symmetry equivalent generated from atom O21 by the operator $(1 + x, y, z)$. The difference map computed with atom H210 omitted from the structure-factor calculation is shown as a wire mesh.

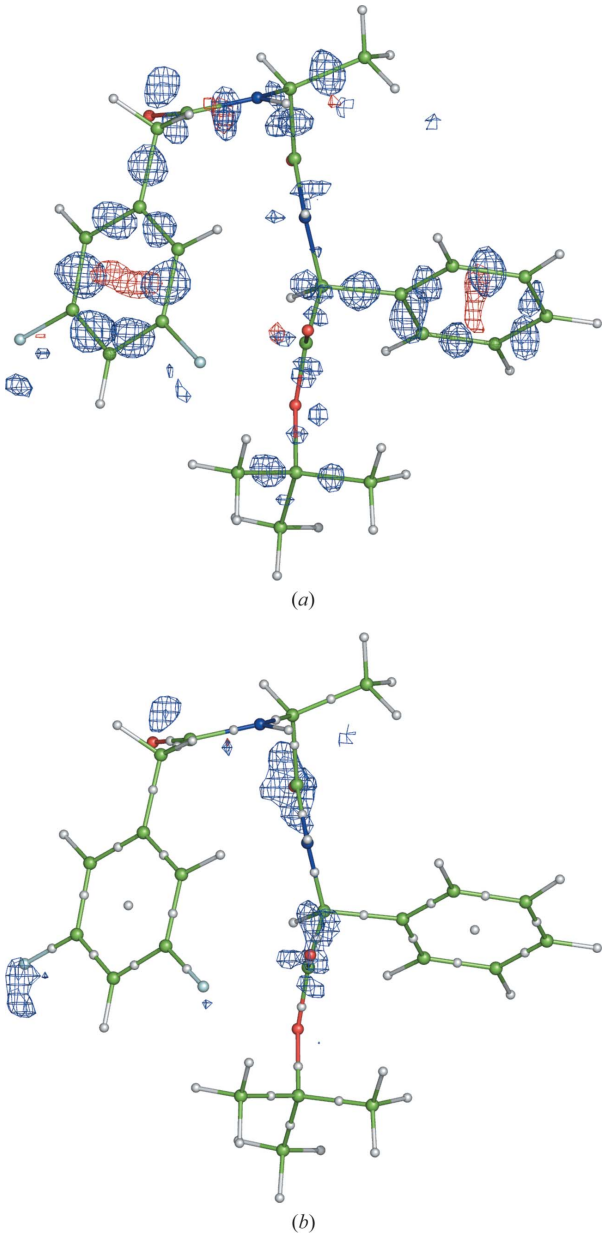

Figure 3
(*a*) Difference Fourier map at 0.11/−0.15 e Å^{-3} contour levels (in the electronic version of the paper, blue denotes positive and red negative) before modeling interatomic scatterers in *PHENIX*. (*b*) Difference Fourier map after IAS refinement at the same contour levels. The positions of the interatomic scatterers (at the centers of the bonds and phenyl rings) are marked as spheres of arbitrary radii, in addition to all atoms.

refinement was attempted where the only difference was that a riding model (of the same character as previously with *SHELXL*) was used for the H atoms instead of refining them freely. Refinement using a riding model resulted in an increased *R*(all) value of 0.0444. The model-phased residual ($F_{obs} - F_{calc}$) map computed for the best IAM model (with H atoms refined freely) showed significant positive electron-density peaks around covalent bond centers for almost all bonds, as well as negative stick-like electron-density blobs at the centers of the aromatic rings oriented perpendicular to the

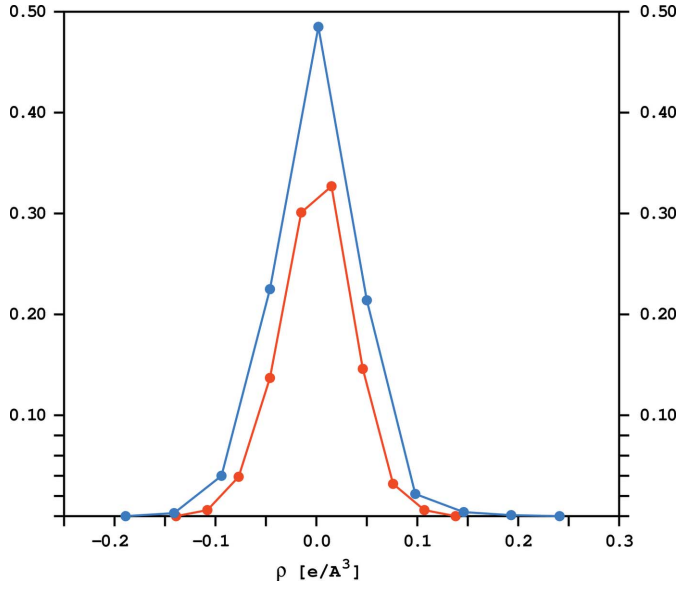

Figure 4
The distribution of the values of the residual difference map before (upper curve) and after (lower curve) the introduction of IAS into the refined model. The graph shows the fraction of map grid points within ten ranges of the density values in the whole map.

ring plane (Fig. 3*a*). These features were accounted for by the addition of IAS to those bonds that showed pronounced residual electron density, and their occupancies and isotropic displacement parameters were refined (anisotropic displacement parameters were refined for aromatic ring-centered IAS). This procedure resulted in *R*(all) = 0.0325 and considerably cleared up the difference density map (Fig. 3*b*). The distribution of the values of the grid points of this map is shown in Fig. 4. Before the introduction of IAS, the map values ranged between −0.214 and 0.266 eÅ^{-3} (r.m.s.d. = 0.063 e Å^{-3}), and afterwards the map was flatter with a range of values between −0.155 and 0.154 e Å^{-3} (r.m.s.d. = 0.037 e Å^{-3}). The results of the *PHENIX* refinement should be treated as final, but are presented in the *Supplementary Material*, since the refined parameters are not accompanied by standard uncertainties.

Experimental

DAPT was prepared according to the general synthetic procedure reported by Kan *et al.* (2004), and a 64% overall yield was obtained. The crude product was purified using preparative high-pressure liquid chromatography, followed by crystallization from a 1:1 mixture of acetonitrile and water.

A needle-like crystal of (I) elongated along *a* was selected, picked up in a rayon loop and quickly cryo-cooled in a stream of cold nitrogen gas at the single-axis goniostat of the SERCAT synchrotron station 22ID at the Advanced Photon Source, Argonne National Laboratory, USA. Diffraction images were collected using a Mar-research MAR300 CCD detector in four passes differing in their effective exposure and resolution limits, in order to measure adequately the weakest high-resolution reflections as well as the strongest low-angle reflections without overloading the detector

Table 1
Hydrogen-bond geometry (Å, °).

D—H···A	D—H	H···A	D···A	D—H···A
N20—H201···O21^{i}	0.92 (4)	2.03 (3)	2.933 (3)	165 (3)

Symmetry code: (i) $x+1, y, z$.

pixels. All 53285 measured intensities from all passes were scaled and merged together into the set of 3216 unique reflections with an overall R_{merge} factor of 0.061. The data set is rather strong, with an $I/\sigma(I)$ ratio of 38 at the highest resolution of 0.72 Å.

Crystal data

$C_{23}H_{26}F_2N_2O_4$
M_r = 432.46
Orthorhombic, $P2_12_12_1$
a = 5.490 (5) Å
b = 15.720 (15) Å
c = 24.82 (2) Å
V = 2142 (4) Å^3
Z = 4
Synchrotron radiation
λ = 0.70000 Å
μ = 0.10 mm^{-1}
T = 100 K
0.25 × 0.05 × 0.04 mm

Data collection

Marresearch MAR300 CCD diffractometer
Absorption correction: multi-scan (*SCALEPACK*; Otwinowski *et al.*, 2003)
T_{min} = 0.974, T_{max} = 0.996
3216 measured reflections
3216 independent reflections
3157 reflections with $I > 2\sigma(I)$
R_{int} = 0.061

Refinement

$R[F^2 > 2\sigma(F^2)]$ = 0.040
$wR(F^2)$ = 0.112
S = 1.10
3216 reflections
384 parameters
All H-atom parameters refined
$\Delta\rho_{max}$ = 0.35 e Å^{-3}
$\Delta\rho_{min}$ = −0.23 e Å^{-3}

The H atoms were located in a difference synthesis and refined without restraints.

The *PHENIX* (Afonine *et al.*, 2005) refinement was performed using a direct summation algorithm for structure-factor and gradient calculation (as opposed to using a fast Fourier transform) and using a maximum-likelihood refinement target (Lunin *et al.*, 2002). Waasmaier & Kirfel (1995) approximation to the standard form factors was used. The form factors for IAS are distributed as part of cctbx (Grosse-Kunstleve *et al.*, 2002).

Data collection: *SERGUI* (SERCAT APS beamline software); cell refinement: *HKL-2000* (Otwinowski & Minor, 1997); data reduction: *HKL-2000*; program(s) used to solve structure: *SHELXD* (Sheldrick, 2008); program(s) used to refine structure: *SHELXL97* (Sheldrick, 2008); molecular graphics: *ORTEP-3* (Farrugia, 1997) and *pyMOL* (DeLano, 2002); software used to prepare material for publication: *ORTEP-3* and *pyMOL*.

Richard Gildea and Luc Bourhis are thanked for their help with using smtbx tools. This work was funded in part with federal funds from the National Cancer Institute under contract No. NO1-CO-12400. The X-ray data were collected at the SERCAT 22ID beamline of the Advanced Photon Source, Argonne National Laboratory; use of the APS was supported by the US Department of Energy under contract No. W-31-109-Eng-38.

Supplementary data for this paper are available from the IUCr electronic archives (Reference: MX3037). Services for accessing these data are described at the back of the journal.

References

Afonine, P. V., Grosse-Kunstleve, R. W. & Adams, P. D. (2005). *CCP4 Newslett.* **42**, contribution 8.
Afonine, P. V., Grosse-Kunstleve, R. W., Adams, P. D., Lunin, V. Y. & Urzhumtsev, A. (2007). *Acta Cryst.* D**63**, 1194–1197.
Afonine, P. V., Lunin, V. Y., Muzet, N. & Urzhumtsev, A. (2004). *Acta Cryst.* D**60**, 260–274.
Barten, D. M., Meredith, J. E., Zaczek, R., Houston, J. G. & Albright, C. F. (2006). *Drugs R D*, **7**, 87–97.
Bittner, T., Fuhrmann, M., Burgold, S., Jung, C. K. E., Volbracht, C., Steiner, H., Mitteregger, G., Kretzschmar, H. A., Haass, C. & Herms, J. (2009). *J. Neurosci.* **29**, 10405–10409.
Chapman, P. F., Falinska, A. M., Knevett, S. G. & Ramsay, M. F. (2001). *Trends Genet.* **17**, 254–261.
DeLano, W. L. (2002). *The pyMOL Molecular Graphics System*. DeLano Scientific, San Carlos, CA, USA.
Dovey, H. F., *et al.* (2001). *J. Neurochem.* **76**, 173–181.
Farrugia, L. J. (1997). *J. Appl. Cryst.* **30**, 565.
Goedert, M. & Spillantini, M. G. (2006). *Science*, **314**, 777–781.
Grosse-Kunstleve, R. W., Sauter, N. K., Moriarty, N. W. & Adams, P. D. (2002). *J. Appl. Cryst.* **35**, 126–136.
Grottkau, B. E., Chen, X., Friedrich, C. C., Yang, X., Jing, W., Wu, Y., Cai, X., Liu, Y., Huang, Y. & Lin, Y. (2009). *Int. J. Oral Sci.* **1**, 81–89.
Hansen, N. K. & Coppens, P. (1978). *Acta Cryst.* A**34**, 909–921.
Hansson, E. M., Lendahl, U. & Chapman, G. (2004). *Semin. Cancer Biol.* **14**, 320–328.
Huang, Y., Yang, X., Wu, Y., Jing, W., Cai, X., Tang, W., Liu, L., Liu, Y., Grottkau, B. E. & Lin, Y. (2010). *Cell Prolif.* **43**, 147–156.
Kan, T., Tominari, Y., Rikimaru, K., Morohashi, Y., Natsugari, H., Tomita, T., Iwatsubo, T. & Fukuyama, T. (2004). *Bioorg. Med. Chem. Lett.* **14**, 1983–1985.
Katoh, M. & Katoh, M. (2007). *Int. J. Oncol.* **30**, 247–251.
Lanz, T. A., Himes, C. S., Pallante, G., Adams, L., Yamazaki, S., Amore, B. & Merchant, K. M. (2003). *J. Pharmacol. Exp. Ther.* **305**, 864–871.
Loane, D. J., Pocivavsek, A., Moussa, C., Thompson, R., Matsuoka, Y., aden, A. I., Rebeck, G. W. & Burns, M. P. (2009). *Nat. Med.* **15**, 377–379.
Lunin, V. Y., Afonine, P. V. & Urzhumtsev, A. G. (2002). *Acta Cryst.* A**58**, 270–282.
Meents, A., Dittrich, B. & Gutmann, S. (2009). *J. Synchrotron Rad.* **16**, 183–190.
Morohashi, Y., Kan, T., Tominari, Y., Fuwa, H., Okamura, Y., Watanabe, N., Sato, C., Natsugari, H., Fukuyama, T., Iwatsubo, T. & Tomita, T. (2006). *J. Biol. Chem.* **281**, 14670–14676.
Otwinowski, Z., Borek, D., Majewski, W. & Minor, W. (2003). *Acta Cryst.* A**59**, 228–234.
Otwinowski, Z. & Minor, W. (1997). *Methods in Enzymology*, Vol. 276, *Macromolecular Crystallography*, Part A, edited by C. W. Carter Jr & R. M. Sweet, pp. 307–326. New York: Academic Press.
Roberts, S. B. (2002). *Adv. Drug Deliv. Rev.* **54**, 1579–1588.
Schmidt, B., Baumann, S., Braun, H. A. & Larbig, G. (2006). *Curr. Top. Med. Chem.* **6**, 377–392.
Sheldrick, G. M. (2008). *Acta Cryst.* A**64**, 112–122.
Sjolund, J., Johansson, M., Manna, S., Norin, C., Pietras, A., Beckman, S., Nilsson, E., Ljungberg, B. & Axelson, H. (2008). *J. Clin. Invest.* **118**, 217–228.
Tomita, T. (2008). *Naunyn-Schmiedeberg's Arch. Pharmacol.* **377**, 295–300.
Vassar, R. (2002). *Adv. Drug Deliv. Rev.* **54**, 1589–1602.
Waasmaier, D. & Kirfel, A. (1995). *Acta Cryst.* A**51**, 416–431.
Wolfe, M. S. (2008). *Curr. Alzheimer Res.* **5**, 158–164.
Zhu, F., Li, T., Qiu, F., Fan, J., Zhou, Q., Ding, X., Nie, J. & Yu, X. (2010). *Am. J. Pathol.* **176**, 650–659.